DOI: 10.1002/chem.200700778

Vesicles of a New Salt-Free Cat-anionic Fluoro/Hydrocarbon Surfactant System

Xin Li,[a] Shuli Dong,[a] Xiangfeng Jia,[a] Aixin Song,[a] and Jingcheng Hao*[a, b]

Abstract: Weakly basic tetradecyldimethylaminoxide (C_{14}DMAO) molecules can be protonated to form a cationic surfactant, $C_{14}DMAOH^+$, by an acidic fluorocarbon surfactant, an 8-2-fluorotelomer unsaturated acid ($C_7F_{15}CF$=CHCOOH), to form a salt-free cationic and anionic (cat-anionic) fluoro/hydrocarbon surfactant system in aqueous solution. The high Krafft point of C_7F_{15}CF=CHCOOH was largely reduced as a result of being mixed with a C_{14}DMAO micelle solution. A study of the phase behavior of the new salt-free cat-anionic fluoro/hydrocarbon surfactant system clearly indicates the existence of a birefringent Lα-phase region at (25.0 ± 0.1) °C. The birefringent Lα phase consists of vesicles, which include uni- and multilamellar vesicles with one to dozens of shells, and oligovesicular vesicles, as demonstrated by freeze-fracture and cryo-transmission electron microscopy (FF- and cryo-TEM) images. The size distribution and structural transitions in the salt-free cat-anionic fluoro/hydrocarbon surfactant system were studied by dynamic light scattering (DLS) and ^{1}H and ^{19}F NMR spectroscopy. The formation of a salt-free cat-anionic vesicle phase could be induced by the strong electrostatic interaction between the cationic hydrocarbon $C_{14}DMAOH^+$ and the anionic fluorocarbon $C_7F_{15}CF$=$CHCOO^-$, which provided evidence that the electrostatic interaction between the cationic and anionic surfactants is larger than the nonsynergistic interaction between the stiff fluorocarbon and the soft hydrocarbon chains of the surfactants.

Keywords: electron microscopy · electrostatic interactions · salt-free solutions · surfactants · vesicles

Introduction

Vesicles[1] formed from amphiphilic molecules in aqueous solutions are fascinating, interesting, and important self-assembled structures with wide-ranging applications in research and as simple model systems for biological membranes.[1a] Since vesicles made of phospholipids, such as lecithin, were first observed in biological systems,[1b] many routes have been explored to construct vesicles by using surfactants in aqueous solution.[1c] Based on the general geometrical considerations of the packing of molecules into distinct aggregate shapes, surfactants can form bilayer membranes when the packing parameter P is in the range of $^1/_2 \leqq P \leqq 1$ ($P=\frac{v}{al}$, in which a is the interfacial area occupied by a surfactant head group and l and v are the length and the volume of the hydrophobic group, respectively).[2] The driving forces for the formation of self-assembled surfactants include van der Waals and hydrophobic forces, hydrogen bonding, and screened electrostatic interactions.[3]

Cationic/anionic (cat-anionic) surfactant mixed systems in aqueous solution are interesting and have been widely studied.[4] There are three main features of cat-anionic systems: 1) Cat-anionic systems are often constructed by mixing a cationic and an anionic hydrocarbon surfactant in aqueous solution, but cat-anionic fluoro/hydrocarbon mixtures have been little studied; 2) the electrostatic interaction of the oppositely charged surfactants significantly reduces the area of the head groups, which produces novel solution and interfacial properties, for example, aggregates can form at considerably lower concentrations than the cricical micelle concentration (CMC) values of each individual surfactant; and 3) traditionally in cat-anionic surfactant mixtures, by using a cationic surfactant with a negatively charged ion, such as Br^- or Cl^-, as the counterion and an anionic surfactant with a positively charged ion, such as Na^+, K^+, or NH_4^+, as the

[a] X. Li, S. Dong, X. Jia, Dr. A. Song, Prof. Dr. J. Hao
Key Laboratory of Colloid and Interface Chemistry
Shandong University, Ministry of Education
Jinan 250100 (China)
Fax: (+86) 531-8856-4750
E-mail: jhao@sdu.edu.cn

[b] Prof. Dr. J. Hao
State Key Laboratory of Solid Lubrication
Lanzhou Institute of Chemical Physics
Chinese Academy of Sciences
Lanzhou 730000 (China)

counterion, the counterions remain in solution to induce high conductivity. The excess salts screens the electrostatic interaction between the cationic and anionic surfactants.[4,5]

Recently it was found that "true", salt-free cat-anionic surfactant mixtures could be constructed by using OH^- and H^+ as the counterions for the cationic and anionic surfactants, respectively, which combine to form water. In particular, self-assembled structures, such as disk-like micelles and regular hollow icosahedral aggregates, in true salt-free aqueous cat-anionic surfactant solutions have been observed by freeze-fracture transmission electron microscopy (FF-TEM), small-angle X-ray scattering (SAXS), and small-angle neutron scattering (SANS).[6–8] Focusing on vesicle formation, we have developed three ways to prepare a charged vesicle phase that is not shielded (salt-free cat-anionic surfactant systems): 1) By adding small amounts of ionic surfactants to the L_3 phase of nonionic surfactants and cosurfactants[9] (it is theoretically argued that the vesicle phase is formed in these systems by the influence of charge density on the Gaussian bending constant[10]); 2) by mixing a cationic surfactant with OH^- as the counterion and an anionic one with H^+ as the counterion, but with one of the two components in small excess;[6–8,11] and 3) by metal–ligand coordination, that is, by mixing an anionic surfactant with M^{2+} (M^{2+} = Zn^{2+}, Ca^{2+}, Ba^{2+}, etc.) as the counterion and coordinated surfactants to form a charged vesicle phase without any cosurfactant and with the charges not shielded because the solutions are salt-free. The vesicle phase was induced by M^{2+}–ligand coordination, in which M^{2+} is the central ion and forms charged bilayers without counterions in the mixtures.[12–14]

Herein we report the construction of a new salt-free cat-anionic vesicle phase in aqueous solution from an unsaturated fluorocarbon carboxylic surfactant, $C_7F_{15}CF{=}CHCOOH$, mixed with a weakly basic surfactant, $C_{14}DMAO$. $C_{14}DMAO$ molecules were protonated to form the cationic surfactant $C_{14}DMAOH^+$ by the unsaturated fluorocarbon carboxylic surfactant $C_7F_{15}CF{=}CHCOOH$.

The structures and properties of the L_1 phase (micelle solution) and the birefringent Lα phase (vesicle phase) were determined by cryo-TEM, FF-TEM, dynamic light scattering (DLS), ^1H and ^{19}F NMR spectroscopy, and rheological measurements. The new salt-free cat-anionic fluoro/hydrocarbon surfactant system is derived from our previous system that involved mixtures of $C_{14}DMAO$ and dihydroperfluorooctanoic acid ($C_6F_{13}CH_2COOH$).[15] In our previous work, we demonstrated that in many cases vesicles do not form spontaneously in aqueous solutions of cat-anionic surfactants, but may be the result of the shear forces that result from mixing the components. We observed the classic Lα phase with stacked bilayers formed by a chemical reaction in situ. The lamellar phase can easily be transformed into vesicles under shearing forces. In this paper we show that uni- and multilamellar vesicles with one to dozens of shells and oligovesicular vesicles are formed by mixing the salt-free cat-anionic fluoro/hydrocarbon surfactant system of $C_{14}DMAO$ and $C_7F_{15}CF{=}CHCOOH$ in aqueous solution.

There were two purposes of this study, first, to prepare true salt-free cat-anionic fluoro/hydrocarbon surfactant mixtures with an ionically charged vesicle phase that is not shielded by excess salt in aqueous solutions, which proves to be valuable and stimulating to fellow specialists, not least because true cat-anionic surfactant systems do not appear to have been exhaustively investigated. Second, to construct a cat-anionic fluoro/hydrocarbon vesicle phase to demonstrate that the electrostatic interaction between cationic and anionic surfactants is larger than the nonsynergistic interaction of the stiff fluorocarbon and the soft hydrocarbon chains of the surfactants.

Results and Discussion

Phase behavior of the $C_{14}DMAO/C_7F_{15}CF{=}CHCOOH$ system: $C_{14}DMAO$ in water can form micelles that have a low viscosity. The solubility of $C_7F_{15}CF{=}CHCOOH$ in water at room temperature is low because $C_7F_{15}CF{=}CHCOOH$ has a high Krafft point ($T_k \approx 55\,°C$), as determined by differential scanning calorimetery (DSC) measurements, which results in simple phase behavior for $C_7F_{15}CF{=}CHCOOH$ in water at room temperature. When different amounts of $C_7F_{15}CF{=}CHCOOH$ were added to a $C_{14}DMAO$ micelle solution, the phase behavior was very interesting. For a $C_{14}DMAO$ micelle solution (100 mmol L^{-1}) mixed with increasing concentrations of $C_7F_{15}CF{=}CHCOOH$, the solutions are thermodynamically stable up to a mole fraction (x_{CF}) of 0.444 ($\approx$78 mmol L^{-1} $C_7F_{15}CF{=}CHCOOH$), as calculated by using Equation (1):

$$x_{CF} = \frac{[C_7F_{15}CF{=}CHCOOH]}{[C_7F_{15}CF{=}CHCOOH] + [C_{14}DMAO]} \quad (1)$$

For solutions with an x_{CF} value of 0 to 0.138, one observes a single transparent solution, which is the L_1 phase (micelle solution). Between x_{CF} values of 0.138 and around 0.194, we observed macroscopic phase separation with an Lα phase at the bottom and an isotropic L_1 phase at the top. After the two-phase region, for solutions with x_{CF} values between 0.194 and 0.375, we observed a single transparent birefringent Lα phase that is very stable, slightly turbid, and bluish. The single birefringent Lα phase contains vesicles, which include uni-, multilamellar, oligovesicular vesicles, as determined by cryo- and FF-TEM images. Solutions with mole fractions of $x_{CF} > 0.375$ again separate into two phases. The upper phase is an isotropic L_1 phase and the Lα phase is below. Examples of the phase behavior of the $C_{14}DMAO$/$C_7F_{15}CF{=}CHCOOH$ system at different concentrations of $C_7F_{15}CF{=}CHCOOH$ with and without polarizers are shown in Figure 1.

The phase diagram of the system that contains $C_{14}DMAO$ (100 mmol L^{-1}) and $C_7F_{15}CF{=}CHCOOH$ (various concentrations), which includes conductivity and pH measurements, is shown in Figure 2. For the $C_{14}DMAO$ micellar solution (100 mmol L^{-1}), one can observe the L_1 phase from 0 to

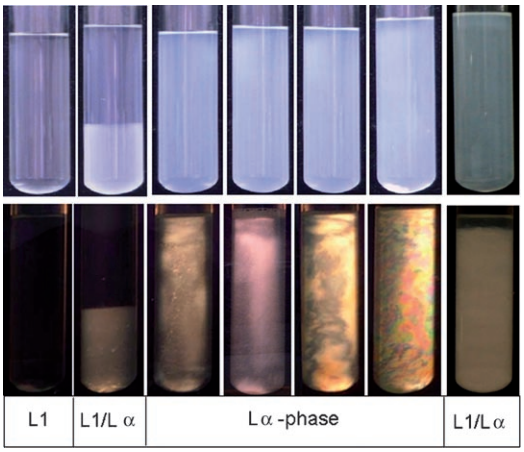

Figure 1. Phase behavior of C_{14}DMAO (100 mmol L^{-1}) with increasing concentrations of C_7F_{15}CF=CHCOOH observed without (top) and with (bottom) polarizers at (25.0±0.1) °C. Concentrations of C_7F_{15}CF=CHCOOH are from left to right 10, 20, 30, 40, 50, 60, and 66 mmol L^{-1}.

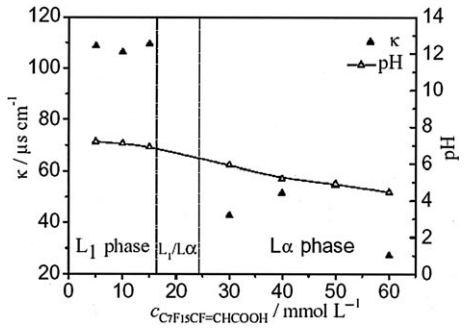

Figure 2. Phase diagram of the system that contains C_{14}DMAO (100 mmol L^{-1}) and C_7F_{15}CF=CHCOOH (various concentrations) at (25.0±0.1) °C. Conductivity and pH changes are included in the phase diagram.

around 16 mmol L^{-1} C_7F_{15}CF=CHCOOH ($x_{CF}=0.138$), the two-phase region between 16 and 24 mmol L^{-1} ($x_{CF}=0.194$), and finally above 24 mmol L^{-1} one can observe the birefringent Lα phase. The conductivity data give clear evidence for the formation of vesicles within the birefringent Lα phase. The vesicles, as demonstrated by the following cryo- and FF-TEM images, enclose part of the solvent and the conductivity ions, and consequently, the number of charge carriers that are in solution and contribute to its conductivity is reduced. As a consequence, the conductivity of the vesicular Lα phase solutions is lowered. However, the pH values decrease gradually in the L_1 and Lα phases as the amount of C_7F_{15}CF=CHCOOH increases.

The Lα phase is birefringent, as demonstrated by the cross-like spherulite textures shown in Figure 3. These textures demonstrate the existence of the lamellar phase.[16]

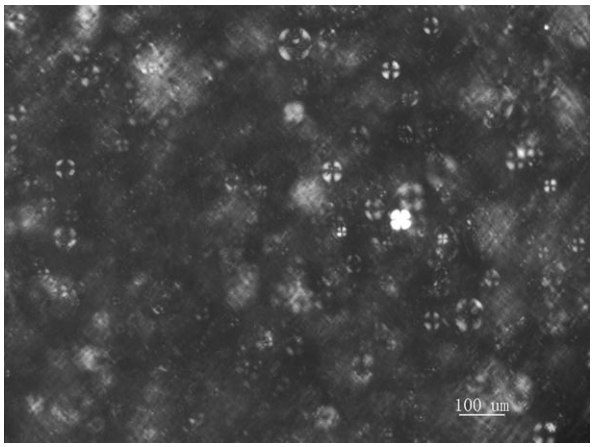

Figure 3. A typical polarized image of the birefringent Lα phase for C_{14}DMAO (100 mmol L^{-1}) and C_7F_{15}CF=CHCOOH (50 mmol L^{-1}) at (25.0±0.1) °C. The scale bar represents 100 μm.

The birefringent Lα phase consists of unilamellar (ULV), multilamellar (MLV), and oligovesicular (OV) vesicles, as shown by the cryo-TEM micrographs in Figure 4. Much information on the vesicles can be obtained from the cryo-TEM images. The multilamellar vesicles located in the top left corner of Figure 4a are clearly tetralamellar. Tri- and bilamellar vesicles can also be easily identified in the cryo-TEM micrographs. Thus, there should be more than one

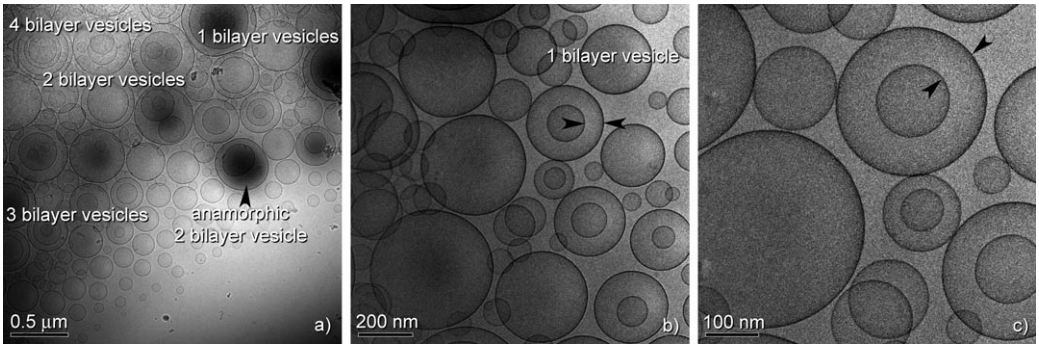

Figure 4. Different magnification cryo-TEM images of the birefringent Lα phase for C_{14}DMAO (100 mmol L^{-1}) and C_7F_{15}CF=CHCOOH (50 mmol L^{-1}) at (25.0±0.1) °C. Multilamellar vesicles can be observed. The interlamellar spacing between the bilayers can be determined by measuring the spacing distribution at different locations of vesicles.

vesicle bilayer and in fact dozens of shells were demonstrated to be present in the FF-TEM images.

The $C_{14}DMAOH^+/^-OOCCH{=}CFC_7F_{15}$ vesicles were characterized by cryo-TEM, which is a technique that allows us to observe vesicle morphology directly without the addition of staining agents. The cryo-TEM micrographs could provide more interesting and significant information. Two types of $C_{14}DMAOH^+/^-OOCCH{=}CFC_7F_{15}$ vesicles could be identified, those that have larger radii or lower curvature and those that smaller radii or higher curvature.[17] Owing to the strongly electron-scattering fluorinated chains, it could be speculated, based on the identical, thick, dark central rings in Figure 4, that the higher the value of x_{CF} the larger the radii or the lower the curvature of the aggregates. The smaller radii or higher curvature vesicles, on the basis of the lighter-shade rings in Figure 4, should have a lower x_{CF} value.[17] Without question, the contrasts in the cryo-TEM images may be due to the different depths of penetration of the electron beam through bilayers of different diameters.

Of course, one could say that a number of vesicle bilayers identified from the cryo-TEM images seem to make contact as a result of electrostatic interactions between the vesicles, that is, the result of a projection of a three-dimensional situation onto a two-dimensional situation. The perfect multibilayer vesicles identified in the high-resolution cryo-TEM images with rather uniform interlamellar spacing of the bilayers could validate vesicle microstructure, that is, the existence of multilamellar vesicles. Cryo-TEM direct imaging provides unambiguous structural information and is perhaps the only method to identify unilamellar vesicles, cylindrical vesicles, discs, worm-like micelles, and so forth, which coexist in a single sample. With careful sample preparation, conservative image interpretation of cryo-TEM images should be made, especially for polydisperse vesicle systems. Additional FF-TEM direct imaging is necessary and a complement to cryo-TEM observations. Different magnification FF-TEM images of the birefringent Lα phase for solutions that contain $C_7F_{15}CF{=}CHCOOH$ (100 and 50 mmol L^{-1}) at (25.0 ± 0.1) °C are shown in Figure 5. As a complement to the cryo-TEM images in Figure 4, FF-TEM images demonstrate that large onions, that is, multilamellar vesicles with one to dozens of shells, not just one to four shells, and oligovesicular vesicles exist.

Some of the vesicles were not easy to categorize because they were oligovesicular. Unilamellar vesicles with diameters ranging from 60 to 400 nm were observed. Small unilamellar vesicles are mainly less than 100 nm in diameter, whereas large ones are more than 200 nm in diameter. The diameters of multi-bilayer vesicles range from 100 to more than 800 nm. The interlamellar spacing of the bilayers is rather uniform and approximately 60 nm.

In the next experiment, we determined the microstructures of the salt-free cat-anionic micelles (L_1 phase) by DLS measurements. Based on the CONTIN method of analysis, Figure 6 shows plots of the intensity contribution function $\Gamma_i G(\Gamma_i)$ versus the apparent hydrodynamic radius (R_h) for three L_1 phase aqueous solutions at different concentrations and scattering angles.

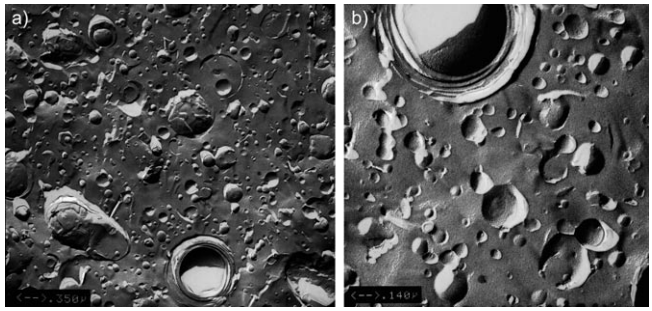

Figure 5. Different magnification FF-TEM images of the birefringent Lα phase for $C_{14}DMAO$ (100 mmol L^{-1}) and $C_7F_{15}CF{=}CHCOOH$ (50 mmol L^{-1}) at (25.0 ± 0.1) °C. Multilamellar and oligovesicular vesicles can clearly be seen in the images. A typical multilamellar vesicle with dozens of shells and a diameter of around 800 nm can be identified in the top of Figure 5b.

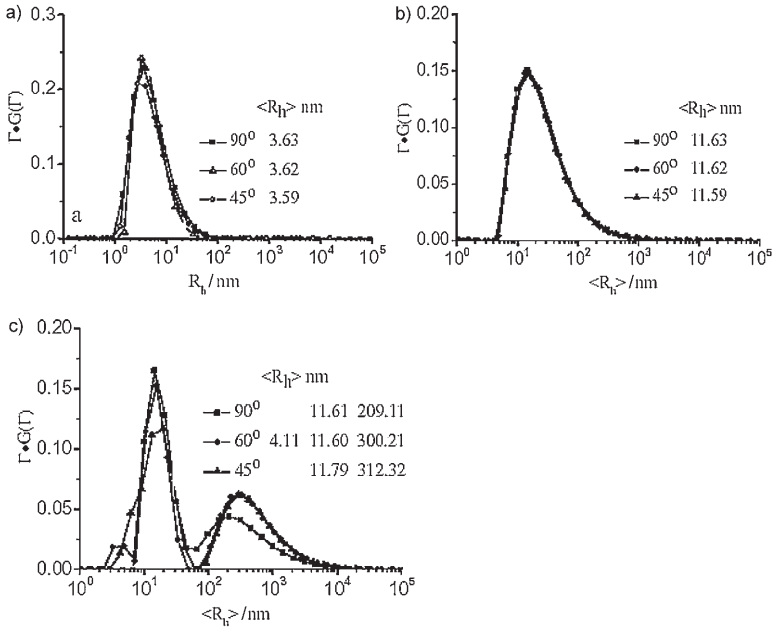

Figure 6. Apparent hydrodynamic radius distributions of three L_1-phase aqueous solutions: a) 100 mmol L^{-1} $C_{14}DMAO$ micelles; b) 100 mmol L^{-1} $C_{14}DMAO$/10 mmol L^{-1} $C_7F_{15}CF{=}CHCOOH$ with mixed spherical and small elliptical; c) 100 mmol L^{-1} $C_{14}DMAO$/15 mmol L^{-1} $C_7F_{15}CF{=}CHCOOH$ with mixed spherical and worm-like micelles.

The aqueous solution of C_{14}DMAO (100 mmol L^{-1}) contains small elliptical micelles,[18] as shown in Figure 6a, in which the size distribution of the micelles consists of only a single distribution with an average hydrodynamic radius $<R_h>$ of about 3.60 nm at different scattering angles and a polydispersity index of $\nu_2/\langle\Gamma\rangle^2 \approx 0.37$. The size distribution of $<R_h>$ is almost the same irrespective of the scattering angle, which implies symmetrical spherical aggregates, that is, spherical C_{14}DMAO micelles.

For a mixture of C_{14}DMAO (100 mmol L^{-1}) and $C_7F_{15}CF$=CHCOOH (10 mmol L^{-1}, Figure 6b), one model is identified at different scattering angles with an average hydrodynamic radius $<R_h>$ of around 11.61 nm with an $\nu_2\langle\Gamma\rangle^2$ value of approximately 0.44. The size distributions show only a small angular independence, which suggest that this mixture has similar aggregates to the previous system, that is, mixed spherical and small elliptical micelles.

For a mixture of C_{14}DMAO (100 mmol L^{-1}) and $C_7F_{15}CF$=CHCOOH (15 mmol L^{-1}, Figure 6c) completely different DLS curves were obtained compared with those of Figure 6a and b. Two models were identified with a scattering angle $\theta = 90°$; $<R_h>$ values of around 11.61 nm with $\nu_2\langle\Gamma\rangle^2 \approx 0.29$ and around 209.11 nm with $\nu_2\langle\Gamma\rangle^2 \approx 0.47$. Three models were identified at $\theta = 60°$; $<R_h>$ values of 4.11 nm with $\nu_2\langle\Gamma\rangle^2 \approx 0.19$, 11.60 nm with $\nu_2\langle\Gamma\rangle^2 \approx 0.28$, and 300.21 nm with $\nu_2\langle\Gamma\rangle^2 \approx 0.49$. Two models were identified at $\theta = 45°$, $<R_h>$ values of 11.79 nm with $\nu_2\langle\Gamma\rangle^2 \approx 0.39$ and 312.32 nm with $\nu_2\langle\Gamma\rangle^2 \approx 0.47$. The first size distribution, having a value of about 4.00 nm, should be the C_{14}DMAO spherical micelles. The second peak with $<R_h> \approx 12.0$ nm corresponds to spherical and small elliptical mixed $C_{14}DMAOH^+/^-OOCCH{=}CFC_7F_{15}$ micelles. The third size distribution should be rod-like mixed micelles.

The macroproperties of the L_1 and the birefringent Lα phases were studied by rheological measurements. Typical rheograms of two L_1-phase samples of 100 mmol L^{-1} C_{14}DMAO and 100 mmol L^{-1} C_{14}DMAO/10 mmol L^{-1} $C_7F_{15}CF$=CHCOOH are shown in Figure 7. The 100 mmol L^{-1} C_{14}DMAO L_1 phase consists of small spherical micelles at (25.0 ± 0.1) °C and behaves like a Newtonian fluid. The apparent viscosity η remains constant with shear rate and shear stress increases proportional to shear rate.

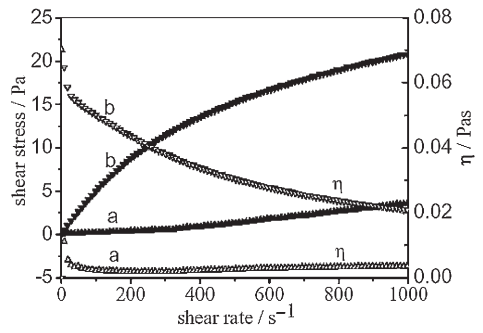

Figure 7. Rheological properties of the L_1 phase: a) 100 mmol L^{-1} C_{14}DMAO and b) 100 mmol L^{-1} C_{14}DMAO/10 mmol L^{-1} $C_7F_{15}CF$=CHCOOH aqueous solutions at (25.0 ± 0.1) °C.

For the L_1 phase of the 100 mmol L^{-1} C_{14}DMAO/10 mmol L^{-1} $C_7F_{15}CF$=CHCOOH system, the flow of the solution changes from Newtonian flow to non-Newtonian flow, which is characterized by a gradual decrease in the apparent viscosity, but the shear stress increases with increasing shear rate.

The birefringent Lα phase of the 100 mmol L^{-1} C_{14}DMAO/50 mmol L^{-1} $C_7F_{15}CF$=CHCOOH aqueous solution has interesting rheological properties. It behaves like a Bingham fluid. The rheological properties of the birefringent Lα phase are completely different to those of the L_1 phase (Figure 7). A typical rheogram of one sample of a birefringent Lα phase is shown in Figure 8. It can be seen that

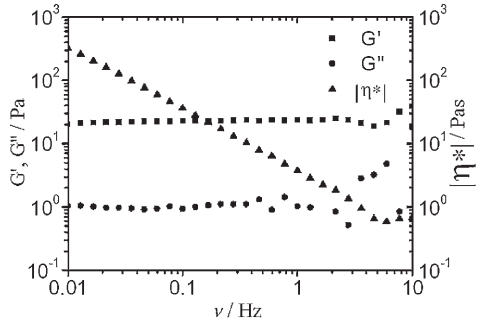

Figure 8. Rheogram of the oscillatory shear for a birefringent Lα-phase sample of 100 mmol L^{-1} C_{14}DMAO/50 mmol L^{-1} $C_7F_{15}CF$=CHCOOH at $T = (25.0 \pm 0.1)$ °C.

the complex fluid behaves like a Bingham fluid with a yield stress value, having the viscoelastic properties, which can be seen by the fact that the storage G' and the loss G'' moduli remain more or less constant at about 22 and 1–2 Pa, respectively, over the whole frequency range investigated. The storage modulus is about one order of magnitude higher than the loss modulus, and the complex viscosities decrease over the whole frequency range from 0.01 to 10 Hz with a slope of −1, which suggests the presence of uni- and multibilayer vesicles.

^{1}H and ^{19}F NMR spectra were recorded by using a Bruker AM-400 spectrometer at (25.0 ± 0.1) °C to monitor the transition between the microstructures in the L_1 and birefringent Lα phases. Typical ^{1}H NMR spectra are shown in Figure 9. In the ^{1}H NMR spectrum of the 100 mmol L^{-1} C_{14}DMAO aqueous solution (in D_2O) (Figure 9a), the stereochemical splitting resonances of α-CH_2, β-CH_2, δ-$(CH_2)_{11}$, ω-CH_3, and ω′-CH_3 are clearly resolved. One can see from the ^{1}H NMR spectrum of the 100 mmol L^{-1} C_{14}DMAO and 10 mmol L^{-1} $C_7F_{15}CF$=CHCOOH L_1-phase solution (Figure 9b) that the addition of $C_7F_{15}CF$=CHCOOH has little effect on the C_{14}DMAO molecules by comparison with the spectrum of the C_{14}DMAO solution in the absence of $C_7F_{15}CF$=CHCOOH.

To compare the ^{1}H NMR results of samples in the L_1 phase, the ^{1}H NMR spectra of samples in the Lα phase were recorded and are shown in Figure 9c and d. The two samples

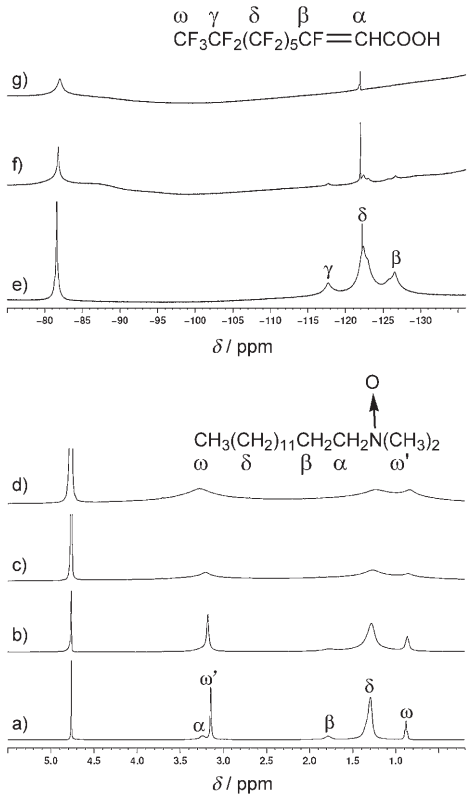

Figure 9. ^{1}H and ^{19}F NMR spectra of the C_{14}DMAO and C_7F_{15}CF=CHCOOH mixed system. ^{1}H NMR spectra: a) 100 mmol L^{-1} C_{14}DMAO L_1 phase (spherical micelles); b) 100 mmol L^{-1} C_{14}DMAO/10 mmol L^{-1} C_7F_{15}CF=CHCOOH L_1 phase; c) 100 mmol L^{-1} C_{14}DMAO/30 mmol L^{-1} C_7F_{15}CF=CHCOOH Lα phase (vesicles), and d) 100 mmol L^{-1} C_{14}DMAO/50 mmol L^{-1} C_7F_{15}CF=CHCOOH Lα phase (vesicles). ^{19}F NMR spectra: e) 100 mmol L^{-1} C_{14}DMAO/10 mmol L^{-1} C_7F_{15}CF=CHCOOH L_1 phase; f) 100 mmol L^{-1} C_{14}DMAO/30 mmol L^{-1} C_7F_{15}CF=CHCOOH Lα phase (vesicles), and g) 100 mmol L^{-1} C_{14}DMAO/50 mmol L^{-1} C_7F_{15}CF=CHCOOH Lα phase (vesicles).

of 100 mmol L^{-1} C_{14}DMAO mixed with 30.0 and 50.0 mmol L^{-1} C_7F_{15}CF=CHCOOH form the birefringent and viscoelastic Lα phase. The ^{1}H NMR spectra of the Lα-phase samples clearly show considerable signal-broadening, which occurs for two reasons. First, the signal-broadening in the ^{1}H NMR spectra could be as a result of incomplete motional narrowing in the birefringent Lα phase. Second, it could be a result of the interaction between C_{14}DMAO and C_7F_{15}CF=CHCOOH owing to electrostatic interactions. Usually, the strong interaction between cationic and anionic surfactants in aqueous solutions induces a large reduction in the area of each head group as a result of ion pairing, which is responsible for the formation of molecular bilayers at low concentrations. In the correct ratios, vesicles may be established spontaneously and are thermodynamically stable species.[19–21] Herein, by using ^{1}H NMR spectroscopy, we have demonstrated the strong interaction between cationic C_{14}DMAOH$^+$ formed by protonation and anionic C_7F_{15}CF=CHCOO$^-$ in the vesicle phase.

The strong interaction between cationic C_{14}DMAOH$^+$ and anionic C_7F_{15}CF=CHCOO$^-$ in the Lα phase (vesicles) has also been demonstrated by ^{19}F NMR spectroscopy (Figure 9). For the L_1-phase sample with C_{14}DMAO (100 mmol L^{-1}) and C_7F_{15}CF=CHCOOH (10 mmol L^{-1}), (Figure 9e), the strong interaction between cationic C_{14}DMAOH$^+$ and anionic C_7F_{15}CF=CHCOO$^-$ produces considerable signal-broadening in the ^{19}F NMR spectra. Only the broadened signals of the ω-CF_3 and δ-$(CF_2)_5$ groups can be observed in the ^{19}F NMR spectra of the two samples in the Lα phase (Figure 9f and g). Other groups such as β-CF and γ-CF_2 do not appear in the ^{19}F NMR spectra, which could mean that the interaction occurs between the head groups of C_{14}DMAOH$^+$ and C_7F_{15}CF=CHCOO$^-$ as a result of electrostatic attraction. The formation of vesicles shows that the electrostatic interaction between cationic C_{14}DMAOH$^+$ and anionic C_7F_{15}CF=CHCOO$^-$ is larger than the nonsynergistic interaction between the stiff fluorocarbon and the soft hydrocarbon chains of the surfactants.

For the C_{14}DMAO (100 mmol L^{-1}) L_1-phase solution we detected spherical micelles by DLS measurements, but small elliptical micelles were also monitored.[18] We have observed the transition between different phase structures induced by the addition of acidic fluorocarbon surfactant to the C_{14}DMAO solution. Vesicles of salt-free cat-anionic C_{14}DMAOH$^+$–$^-$OOCCH=CFC_7F_{15} surfactants were prepared. One can assume that the addition of C_7F_{15}CF=CHCOOH to a solution of C_{14}DMAO should increase the packing parameter because C_{14}DMAO can be protonated by C_7F_{15}CF=CHCOOH to form cationic C_{14}DMAOH$^+$. It is supposed that the acid–base reaction in Equation (2) occurs between C_{14}DMAO and C_7F_{15}CF=CHCOOH to form a salt-free cat-anionic surfactant mixture. The salt-free cat-anionic surfactant mixture formed by attractive interactions between C_{14}DMAOH$^+$ and C_7F_{15}CF=CHCOO$^-$ should be responsible for the formation of vesicles.

$$C_{14}DMAO + HOOCCH{=}CFC_7F_{15} \rightarrow C_{14}DMAOH^+ - {}^-OOCCH{=}CFC_7F_{15} \quad (2)$$

Conclusion

For a C_{14}DMAO (100 mmol L^{-1}) L_1-phase solution one observes an isotropic L_1 phase, a two-phase L_1/Lα system, and a birefringent Lα phase by increasing the concentration of C_7F_{15}CF=CHCOOH in solution. A birefringent Lα phase that consists of unilamellar vesicles, multilamellar vesicles with one to dozens of shells, and oligovesicular vesicles were prepared in a mixture of weakly basic C_{14}DMAO and acidic C_7F_{15}CF=CHCOOH. The formation of vesicles shows that the electrostatic interaction between cationic C_{14}DMAOH$^+$ and anionic C_7F_{15}CF=CHCOO$^-$ is larger than the nonsynergistic interaction between the stiff fluorocarbon and the soft hydrocarbon chains of the surfactants.

Experimental Section

Chemicals: The unsaturated 8-2-fluorotelomer acid $C_7F_{15}CF{=}CHCOOH$ ($M_W = 458.1\,g\,mol^{-1}$, melting point: 101.5–104.5 °C) was a gift from Hoechst Aktiengesellschaft Werk, Gendorf (Frankfurt-am-Main, Germany) and was used without further purification. Tetradecyldimethylaminoxide ($C_{14}DMAO$) was a gift of Clariant AG, Gendorf (Frankfurt-am-Main, Germany) and was delivered as a 25 wt% solution. It was crystallized twice from acetone and characterized by its melting point (130.2–130.5 °C) and c.m.c. (1.4×10^{-4} mol L^{-1}).

Methods: Different amounts of $C_7F_{15}CF{=}CHCOOH$ were added to a $C_{14}DMAO$ micellar solution (100 mmol L^{-1}), which has a zero-shear viscosity $|\eta^0|$ of 1.98×10^{-3} Pas, a conductivity κ of 49.40 μS cm^{-1}, and pH 8.40. The mixed sample solutions were homogenized by shaking and then thermostatted at (25.0 ± 0.1) °C for 3 to 4 months to reach equilibrium. Preliminary studies involved visual inspection either with or without crossed polarizers to verify the homogeneity and birefringence of the samples. Polarizing optical microscopy measurements of birefringent samples were performed by using a Carl Zeiss Axioskop 40 light microscope (Germany). The pH values and conductivities of the samples were measured with a PHS-3C pH meter and a DDSJ-308A conductivity meter, respectively.

The rheological measurements were performed with a HAAKE RheoStress RS75 instrument. The magnitudes of the complex viscosity $|\eta^*|$, the storage modulus G', and the loss modulus G'' were measured in a frequency range of 0.01–10 Hz.

To prepare dust-free solutions for DLS measurements, the sample solutions were filtered directly into dust-free light-scattering cells through Millipore sterile membrane filters depending on the concentrations and the sizes of the aggregates. The light-scattering cells were rinsed inside and out with distilled (dust-free) acetone to ensure dust-free conditions before use. A standard Brookhaven Commercial laser light-scattering spectrometer equipped with a coherent radiation 200 mW diode-pumped solid-state (DPPS) 488 laser operating at 488 nm and a Brookhaven Instruments Corporation (BI-9000 AT) correlator was used in the DLS measurements. The spectrometer is capable of measuring both the angular dependence of the absolute integrated scattered intensity over a scattering angular range of 20–140° and the intensity–intensity digital photon correlation over a similar angular range (DLS and dynamic depolarization light scattering). About 2–3 mL of the sample solutions were transferred into scattering cells for light scattering measurements. The scattering cells were held in a brass thermostat block filled with silicone oil with a matching refractive index. The temperature was controlled to within ±0.05 °C.

DLS measures the intensity–intensity time correlation function $G^{(2)}(\Gamma)$ in the self-beating mode where Γ is the characteristic line-width. $G^{(2)}(\Gamma)$ can be related to the electric field time correlation function $g^{(1)}(\tau)$ given by Equation (3), in which A and b are the background (baseline) and a coherence factor (a parameter depending on the detection coherence), respectively. The electric field time correlation function $g^{(1)}(\tau)$ was analyzed by the constrained regularized CONTIN method[22,23] to yield the characteristic line-width distribution $G(\Gamma)$ by inversion of Equation (4).

$$G^{(2)}(\Gamma) = A(1 + b|g^{(1)}(\tau)|^2) \tag{3}$$

$$|g^{(1)}(\tau)| = \int_0^\infty G(\tau)e^{-\Gamma\tau}\mathrm{d}\Gamma \tag{4}$$

The first and second moments of $G(\Gamma)$ are $<\Gamma> = \int_0^\infty \Gamma G(\Gamma)\mathrm{d}\Gamma$ and $\nu_2 = \int_0^\infty (\Gamma - <\Gamma>)^2 G(\Gamma)\mathrm{d}\Gamma$, respectively. The value of $\nu_2/<\Gamma>$ is a measure of the particle polydispersity. If the relaxation is diffusive, Γ can be related to the average apparent diffusion coefficient (D) by Equation (5), in which q is the magnitude of the scattering wave vector which is given by Equation (6), in which n_0 is the refractive index of the liquid, λ_0 is the wavelength of the laser in a vacuum (here $\lambda_0 = 532$ nm), and θ is the scattering angle. The apparent hydrodynamic radius R_h can be obtained from the Stokes–Einstein equation [Eq. (7)], in which k_B is the Boltzmann constant and η is the solvent viscosity at temperature T. Based on Equations (4) and (5), a characteristic line-width distribution $G(\Gamma)$ corresponds to a distribution of an apparent hydrodynamic radii from which, for example, the average apparent hydrodynamic radius R_h can be determined. The DLS measurements were performed at finite concentrations and interparticle interactions have been neglected.

$$D = \Gamma/q^2 \tag{5}$$

$$q = \frac{4\pi n_0}{\lambda_0}\sin\frac{\theta}{2} \tag{6}$$

$$R_h = \frac{k_B T}{6\pi\eta \mathrm{D}} \tag{7}$$

Carbon film grids with hole sizes between 1 and 12 mm were used for specimen preparation. A drop of the sample solution was placed on an untreated coated TEM grid (copper grid, 3.02 mm, 200 mesh). Most of the liquid was removed with blotting paper to leave a thin film stretched over the holes. The specimens were instantly shock-frozen by plunging them into liquid ethane in a temperature-controlled freezing unit (Zeiss, Oberkochen, Germany). After freezing the specimens, the remaining ethane was removed by using blotting paper. The specimens were inserted into a cryo-transfer holder (Zeiss, Oberkochen, Germany) and transferred to a Zeiss CEM 902 apparatus equipped with a cryo-stage. Examinations were carried out at a constant temperature of 90 K. TEM was carried out with an accelerating voltage of 80 kV. Zero-loss filtered images ($\Delta E = 0$ eV) were taken under low-dose conditions. To determine the mean lamellarity, micrographs of three different areas of the specimen were used. All vesicles contained within several holes of the carbon film grid were counted to ensure an average count of small and large vesicles.

To characterize and detect the structures of the Lα phase, FF-TEM was carried out. For FF-TEM observations, a small amount (≈4 μL) of sample was placed on a 0.1 mm thick copper disk covered with a second copper disk. The copper sandwich of the sample was frozen in liquid propane cooled by liquid nitrogen in advance. Fracturing and replication were carried out in a freeze-fracture apparatus (Balzer BAF 400, Germany) at a temperature of −140 °C. Pt/C was deposited at an angle of 45°. The replicas were examined by using a JEOL 100cx II TEM instrument (Japan) at an accelerating voltage of 100 kV.

The ^1H and ^{19}F NMR spectra were measured with a Bruker AM-400 spectrometer. The measurements were conducted by using 5 mm NMR sample tubes.

All of the experiments described above were performed at (25.0 ± 0.1) °C.

Acknowledgements

This work was financially supported by the NSFC (Grant No. 20625307, 20533050, and 20473049). We are grateful to Professor Dr. Heinz Hoffmann for discussions and Dr. Markus Drechsler of Bayreuth Universität (Germany) for conducting the cryo-TEM measurements.

[1] a) *"Vesicles" in Surfactant Science Series 62* (Ed.: M. Rosoff), Marcel Dekker, New York, **1996**; b) D. D. Lasic, "*Liposomes: From Physics to Applications*", Elsevier, Amsterdam, **1993**; c) R. G. Laughlin, "*The Aqueous Behavior of surfactants*", Academic press, London, **1994**.

[2] J. Israelachvili, D. J. Mitchell, B. W. Ninham, *J. Chem. Soc., Faraday Trans. 2* **1976**, *72*, 1525.

[3] J. N. Israelachvili, *Intermolecular and surface forces*, 2nd ed., Academic press, New York, **1991**.

[4] J. Hao, H. Hoffmann, *Curr. Opin. Colloid Interface Sci.* **2004**, *9*, 279.

[5] K. Horbaschek, H. Hoffmann, J. Hao, *J. Phys. Chem. B* **2000**, *104*, 2781.

[6] Th. Zemb, M. Dubois, B. Demé, Th. Gulik-Krzywicki, *Science* **1999**, *283*, 816.
[7] M. Dubois, B. Demé, Th. Gulik-Krzywicki, J. C. Dediu, C. Vautrin, S. Désert, E. Perez, Th. Zemb, *Nature* **2001**, *411*, 672.
[8] M. Dubois, V. Lizunov, A. Meister, Th. Gulik-Krzywicki, J. M. Verbavatz, E. Perez, J. Zimmerberg, Th. Zemb, *Proc. Natl. Acad. Sci. USA* **2004**, *101*, 15082.
[9] H. Hoffmann, C. Thunig, P. Schmiedel, U. Munkert, *Langmuir* **1994**, *10*, 3972.
[10] H. N. W. Lekkerkerker, *Physica A (Amsterdam, Neth.)* **1990**, *167*, 384.
[11] a) A. Song, S. Dong, X. Jia, J. Hao, W. Liu, T. Liu, *Angew. Chem.* **2005**, *117*, 4086; *Angew. Chem. Int. Ed.* **2005**, *44*, 4018; b) J. Hao, W. Liu, G. Xu, L. Zheng, *Langmuir*, **2003**, *19*, 10635.
[12] J. Hao, J. Wang, W. Liu, R. Abdel-Rahem, H. Hoffmann, *J. Phys. Chem. B* **2004**, *108*, 1168.
[13] J. Wang, A. Song, X. Jia, J. Hao, W. Liu, H. Hoffmann, *J. Phys. Chem. B* **2005**, *109*, 11126.
[14] A. Song, X. Jia, M. Teng, J. Hao, *Chem. Eur. J.* **2007**, *13*, 496.
[15] J. Hao, H. Hoffmann, K. Horbaschek, *Langmuir* **2001**, *17*, 4151.
[16] K. Horbaschek, H. Hoffmann, C. Thunig, *J. Colloid Interface Sci.* **1998**, *206*, 439.
[17] M. Schmutz, B. Michels, P. Marie, M. P. Krafft, *Langmuir* **2003**, *19*, 4889.
[18] H. Hoffmann, G. Oetter, B. Schwandner, *Prog. Colloid Polym. Sci.* **1987**, *73*, 95.
[19] E. W. Kaler, K. A. Murthy, B. E. Rodriguez, J. A. N. Zasadzinski, *Science* **1989**, *245* 1371.
[20] E. Marques, A. Khan, M. Miguel, B. Lindman, *J. Phys. Chem.* **1993**, *97*, 4729.
[21] M. Bergstrom, J. S. Pedersen, P. Schurtenberger, S. U. Egelhaf, *J. Phys. Chem. B* **1999**, *103*, 9888.
[22] S. W. Provencher, *Biophys. J.* **1976**, *16*, 29.
[23] S. W. Provencher, *J. Chem. Phys.* **1976**, *64*, 2772.

Received: May 23, 2007
Published online: September 11, 2007

